Accepted Manuscript

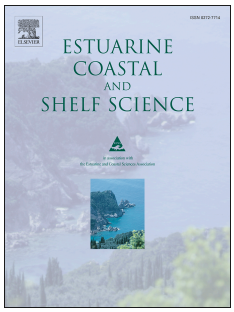

Lagrangian trajectories, residual currents and rectification process in the Northern Gulf of California

Pablo Alonso Rodríguez, Noel Carbajal, Juan Heberto Gaviño Rodríguez

PII: S0272-7714(17)30200-7

DOI: 10.1016/j.ecss.2017.06.019

Reference: YECSS 5509

To appear in: *Estuarine, Coastal and Shelf Science*

Received Date: 18 February 2017

Revised Date: 7 June 2017

Accepted Date: 14 June 2017

Please cite this article as: Rodríguez, P.A., Carbajal, N., Rodríguez, Juan.Heberto.Gaviñ., Lagrangian trajectories, residual currents and rectification process in the Northern Gulf of California, *Estuarine, Coastal and Shelf Science* (2017), doi: 10.1016/j.ecss.2017.06.019.

Lagrangian trajectories, residual currents and rectification process in the Northern Gulf of California

Pablo Alonso Rodríguez

Noel Carbajal

Juan Heberto Gaviño Rodríguez

Abstract

Considering a semi-implicit approximation of the Coriolis terms, a numerical solution of the vertically integrated equations of motion is proposed. To test the two-dimensional numerical model, several experiments for the calculation of Euler, Stokes and Lagrange residual currents in the Gulf of California were carried out. To estimate the Lagrangian residual current, trajectories of particles were also simulated. The applied tidal constituents were M_2, S_2, K_2, N_2, K_1, P_1 and O_1. At spring tides, strong tidal velocities occur in the northern half of the gulf. In this region of complex geometry, depths change from a few meter in the northern shelf zone to more than 3000 m in the southern part. In the archipelago region, the presence of islands alters amplitude and direction of tidal currents producing a rectification process which is reflected in a clockwise circulation around Tiburón Island in the Lagrangian residual current. The rectification process is explained by the superposition of the Euler and Stokes residual currents. Residual current patterns show several cyclonic and anticyclonic gyres in the Northern Gulf of California. Numerical experiments for individual and combinations of several tidal constituents revealed a large variability of Lagrangian trajectories.

Key words

Numerical modelling, Lagrangian trajectories, tides, residual currents, currents rectification

Introduction

Tides in the Gulf of California show a wide range of phenomena as result of the interaction of impressive tides and a complex geometry. The northern part of the gulf can be considered as a shelf with a maximum depth of about 200 m (Figure 1). Intense tidal currents characterize mainly this northern part. In the shallow area of the Colorado River Delta, amplitude ranges reach at spring tides values of about 10 meters and the strong tidal currents achieve values of more than 2 ms^{-1}. The sediments availability combined with the strong currents produce large sediments mobility and the formation of sand banks in the northernmost part of the gulf. In the southern part of the gulf, depths reach values of more than 3000 m. Tidal currents are small in these deep areas, but along the coastal regions, tidal currents are important. In the central part of the Gulf of California, in the transition zone from large depths to shelf conditions, there is an archipelago formed principally by the islands Tiburon and Angel de la Guarda among other smaller landmasses.

One of the first evaluations of ti dal processes in the Gulf of California was carried out by Hendershott and Speranza (1971). They investigated the position of the sea surface elevation amphidromic system of the M_2 tide. They predicted a large dissipation of tidal energy in the northern part through the displacement of the amphidromic point to the side of the reflected Kelvin wave. Filloux (1973) then estimated the dissipation of tidal energy in a tidal cycle of the M_2 tide. He found a value of 4.35 x 10^9 joules s^{-1}. Applying for the first time a numerical model (with a coarse resolution), Grijalva (1972) calculated some aspects of tides like currents, amplitudes and phases. A more sophisticated numerical modelling of tides was carried out by Stock (1976) who gave special importance to tidal dissipation of energy. Using tidal observation around the gulf, cotidal and corange maps of the principal tidal constituents (M_2, S_2, N_2, K_2, O_1, K_1, P_1, Sa, SSa, Mf) were estimated by Morales-Pérez and Gutierrez de Velasco (1989). Quirós et al. (1992) calculated the Euler residual current of the M_2 tide in the Gulf of California applying a vertically integrated numerical model with a grid resolution of 14 km. A similar calculation for

the estimation of the Euler residual currents was carried out by Argote et al. (1995). Carbajal (1993) applied for the first time a three dimensional numerical model to investigate the vertical variation of tidal currents, Euler residual currents, energy budget and baroclinic aspects of tides. These calculations revealed that residual currents are, in general, two orders of magnitude smaller than the instantaneous flow. Marinone and Lavín (2003) calculated residual currents and tidal mixing in the archipelago region. Energy budgets of the M_2 and S_2 tides, the distribution of kinetic energy, the dissipation of energy by bottom friction and turbulent viscosity and the resonance periods of the gulf were estimated by Carbajal and Backhaus (1998). Applying a three-dimensional numerical model, Salas de León et al. (2003) calculated the Euler residual current and the tidal stress generated by the M_2 tidal constituent in the Gulf of California. Tidal stress values were especially high over the Salsipuedes sill, in the Ballenas Channel, in the archipelago region and in the Colorado River Delta. They also found that high tidal stress values coincide well with the anomalous cold-water patches observed in the archipelago area. Using a three-dimensional numerical model, the Lagrangian surface circulation was investigated by Gutiérrez et al. (2004). They calculated the advection of particles for monthly and annual periods by forcing the circulation with the tidal constituents M_2, S_2, N_2, K_2, K_1, P_1, O_1, SSa, Sa. One of the most important finding was that in the northern part of the gulf the circulation is anticyclonic from October to May and cyclonic during the summer months. Salas de Leon et al. (2011) calculated the vorticity and mixing produced by the M_2 tide. They found a connection between the horizontal component of the vorticity and zooplankton biomass distribution in the northern part of the gulf. Tides in the Gulf of California also generate internal waves. Fu and Holt (1984) found that the number of internal wave groups was correlated with the strength of tides in the archipelago region, i.e. the region where the internal waves are generated. The strength of tidal currents in the Gulf of California plays also an important role in the morphodynamics of shallow zones (Montaño and Carbajal, 2008). The observed wave lengths of sandbanks in the Colorado River Delta have been explained with a theoretical model where tidal forcing is considered (Carbajal and Montaño, 2001). The bedload transport of

sediments was estimated in the Colorado River Delta and in the Adair and San Jorge bays (Hernandez-Azcunaga et al., 2013).

Many aspects of tides in the Gulf of California have been investigated like the displacement of amphydromic systems, dissipation of energy by bottom friction, energy budgets, residual currents, intensity of instantaneous flow, vorticity and mixing, connectivity among the different regions of the gulf, bedload transport of sediment, morphodynamics of the sea bottom in shallow areas, tidal stress, Lagrangian trajectories, among other tidal processes. In the present research work, Lagrangian trajectories are applied to estimate residual currents considering several tidal constituents. It is worth mentioning that in many studies, tidal residual currents have been estimated dominantly applying the Euler method. The Lagrange and Stokes residual currents are also suitable to explain important dynamical phenomena like transport of tracers and rectification processes. Since there is an archipelago in the central part of the Gulf of California, it is relevant to investigate the effect of the archipelago on the Lagrange, Euler and Stokes residual currents. In fact, the rectification of tidal currents by the presence of islands is examined using Euler, Stokes and Lagrange residual currents. For the estimation of the Langrange residual current, Lagrangian trajectories and the Euler and Stokes residual currents were applied. The complexity of the Lagrangian trajectories is likewise investigated.

Stability analysis and model

In the numerical approximation of the Coriolis term arises the problem of an increasing radius of the inertial wave. During the applied time step Δt, the velocity vector remains in a tangential direction increasing artificially the orbital motion in a spiral form. To mitigate this numerical problem, several algorithms are used, among them the application of a rotational matrix or a semi-implicit approximation of the Coriolis term. Since a numerical solution of the vertically integrated

equations of motion is presented in this section, a simple stability analysis of these two approximations is carried out. From this analysis, the applied approximation for the Coriolis term and the proposed numerical solution is grounded. The horizontal equations of motion can be written in the simplified form

$$\frac{dV}{dt} + (r + if)V = q \tag{1}$$

Where a linear friction term was considered and the horizontal components of the velocity, (u, v), are projected on a complex plane, i.e. $V = V(u, v) = u + iv$, and $q = q_u + iq_v$, where q represents other terms in the equation of motion. $f = 2\Omega \sin\phi$ is the Coriolis term, ϕ is the latitude, Ω is the angular velocity of Earth and r is the linear friction coefficient. The solution for this differential equation with $q = cte$ is

$$V = e^{-rt}\left(V_0 - V_p\right)\left(\cos ft - i \sin ft\right)\right) + V_p \tag{2}$$

Where $V_0 = V(t = 0)$ and $V_p = \frac{q}{r + ift}$. After some manipulations and considering that $e^{-rt} \approx \frac{1}{1 + rt}$, the solution in components of equation (1) takes the form

$$u = \frac{1}{1 + rt}\left(u_0 \cos ft + v_0 \sin ft + tq_u\right) \tag{3}$$

$$v = \frac{1}{1 + rt}\left(-u_0 \sin ft + v_0 \cos ft + tq_v\right) \tag{4}$$

Use was made of $1 - \cos ft \approx \frac{(ft)^2}{2}$, $|ft| << 1$ and $\sin ft \approx ft$. In the solution, described by equations (3) and (4), the rotation matrix $\begin{pmatrix} \cos ft & \sin ft \\ -\sin ft & \cos ft \end{pmatrix}$ appears, i.e. the rotation matrix is contained in the equations of motion. It explain its application on

the Coriolis term in numerical solutions. A stability analysis of the inertial equations for three approximations, i.e. for a simple approximation, for the application of a rotation matrix and for a semi-implicit treatment of the Coriolis term, is carry out as a next step. The inertial equations

$$\frac{\partial u}{\partial t} + fv = 0 \tag{5}$$

$$\frac{\partial v}{\partial t} - fu = 0 \tag{6}$$

can be numerically approximated in an Arakawa C grid in the following way:

$$u_{k,l}^{n+1} = u_{k,l}^{n} + \frac{f\Delta t\left(v_{k-s,l+p}^{n} + v_{k+s,l+p}^{n} + v_{k-s,l-p}^{n} + v_{k+s,l-p}^{n}\right)}{4} \tag{7}$$

$$v_{k,l}^{n+1} = v_{k,l}^{n} + \frac{f\Delta t\left(u_{k,l}^{n} + u_{k-s,l}^{n} + u_{k,l+p}^{n} + u_{k-s,l+p}^{n}\right)}{4} \tag{8}$$

The variables s and p take the values, $\left(\frac{1}{2},-\frac{1}{2},0\right)$, according to the positions of (u,v) in an Arakawa C mesh. Using the Fourier method for the stability analysis, the variables, (u,v), are represented in the form

$$u_{k+s,l+p}^{n} = u\gamma^{n} e^{i(s\alpha\Delta x + p\beta\Delta y}$$

From (7) and (8), the relations

$$\gamma u = u + \frac{f\Delta t v}{4}\left[\left(e^{-i\alpha\frac{\Delta x}{2}} + e^{i\alpha\frac{\Delta x}{2}}\right)e^{i\beta\frac{\Delta y}{2}} + \left(e^{-i\alpha\frac{\Delta x}{2}} + e^{i\alpha\frac{\Delta x}{2}}\right)e^{-i\beta\frac{\Delta y}{2}}\right] \tag{9}$$

$$\gamma w = v + \frac{f\Delta t u}{4}\left[\left(e^{-i\alpha\frac{\Delta x}{2}} + e^{i\alpha\frac{\Delta x}{2}}\right)e^{i\beta\frac{\Delta y}{2}} + \left(e^{-i\alpha\frac{\Delta x}{2}} + e^{i\alpha\frac{\Delta x}{2}}\right)e^{-i\beta\frac{\Delta y}{2}}\right] \tag{10}$$

were obtained. Applying the equalities for the cosine function, the equations (9) and (10) can be written in the matrix form:

$$\begin{bmatrix} (1-\gamma) & f\Delta t \cos\alpha\frac{\Delta x}{2}\cos\beta\frac{\Delta y}{2} \\ -f\Delta t \cos\alpha\frac{\Delta x}{2}\cos\beta\frac{\Delta y}{2} & (1-\gamma) \end{bmatrix}\begin{bmatrix} u \\ v \end{bmatrix} = \begin{bmatrix} 0 \\ 0 \end{bmatrix}$$

The calculation of the determinant leads to

$$|\gamma| = \left[1 + \left(f\Delta t \cos\alpha\frac{\Delta x}{2}\cos\beta\frac{\Delta y}{2}\right)^2\right]^{\frac{1}{2}} > 1 \tag{11}$$

This numerical approximation of the Coriolis terms is unstable. If a linear friction is included in the inertial equations (5) and (6), then the following stability condition

$$(1 + f\Delta t)^2 \le (1 + r\Delta t) \tag{12}$$

Is obtained. Using a similar stability analysis for the inertial equations but this time applying a rotation matrix, then the stability criterion

$$o \le |\gamma|^2 \le 1 \tag{13}$$

is deduced. The application of a rotation matrix in numerical solutions of the inertial equations is always stable. Another interesting numerical approximation of the inertial equations is the application of a semi-implicit approach. The stability analysis leads in this case to the stability criterion

$$f\Delta t \le 2 \tag{14}$$

If friction is included in the inertial equations then (14) changes to

$$f\Delta t \le 2\left(1+rt\right)^{\frac{1}{2}} \tag{15}$$

This is also a strong stability criterion. This stability analysis for different approaches of the numerical solutions of the inertial equations yields two principal outcomes; there is numerical stability when a rotation matrix is applied and when the Coriolis terms are approximated in a semi-implicit form. The semi-implicit approximation of the Coriolis terms suggests a numerical approach for the solution of the vertically integrated equations of motion. This solution is described below.

Consider the horizontal components of the vertically integrated equations of motion

$$\frac{\partial U}{\partial t}+\frac{U}{H+\zeta}\frac{\partial U}{\partial x}+\frac{V}{H+\zeta}\frac{\partial U}{\partial y}-fV=-g\left(H+\zeta\right)\frac{\partial \zeta}{\partial x}+A_H\left(\frac{\partial^2 U}{\partial x^2}+\frac{\partial^2 U}{\partial y^2}\right)-\frac{rU\sqrt{U^2+V^2}}{\left(H+\zeta\right)^2}$$

(16)

$$\frac{\partial V}{\partial t}+\frac{U}{H+\zeta}\frac{\partial V}{\partial x}+\frac{V}{H+\zeta}\frac{\partial V}{\partial y}+fU=-g\left(H+\zeta\right)\frac{\partial \zeta}{\partial y}+A_H\left(\frac{\partial^2 V}{\partial x^2}+\frac{\partial^2 V}{\partial y^2}\right)-\frac{rV\sqrt{U^2+V^2}}{\left(H+\zeta\right)^2}$$

(17)

Where (U,V) are the transports (m^2/s) in the directions x (west-east) and y (south-north). H is the water depth, ζ is the sea surface elevation, t is the time, A_H is the horizontal eddy viscosity and r is the friction coefficient. The continuity equation is given by

$$\frac{\partial \zeta}{\partial t}+\frac{\partial U}{\partial x}+\frac{\partial V}{\partial y}=0 \tag{18}$$

The equations (16) and (17) can be written in the form

$$\frac{\partial U}{\partial t}=fV-\frac{rU\sqrt{U^2+V^2}}{\left(H+\zeta\right)^2}+T^{(x)} \tag{19}$$

$$\frac{\partial V}{\partial t} = -fU - \frac{rV\sqrt{U^2+V^2}}{(H+\zeta)^2} + T^{(y)} \tag{20}$$

With

$$T^{(x)} = -\frac{U}{H+\zeta}\frac{\partial U}{\partial x} - \frac{V}{H+\zeta}\frac{\partial U}{\partial y} - g(H+\zeta)\frac{\partial \zeta}{\partial x} + A_H\left(\frac{\partial^2 U}{\partial x^2} + \frac{\partial^2 U}{\partial y^2}\right) \tag{21}$$

$$T^{(y)} = -\frac{U}{H+\zeta}\frac{\partial V}{\partial x} - \frac{V}{H+\zeta}\frac{\partial V}{\partial y} - g(H+\zeta)\frac{\partial \zeta}{\partial y} + A_H\left(\frac{\partial^2 V}{\partial x^2} + \frac{\partial^2 V}{\partial y^2}\right) \tag{22}$$

The discretization of the equations (19) and (20) applying a semi-implicit approach for the Coriolis terms is then

$$\frac{U_{i,j}^{n+1} - U_{i,j}^{n}}{\Delta t} = \frac{f_U\left(V_{i,j}^{n+1} + \overline{V}_{i,j}^{n}\right)}{2} - \frac{rU_{i,j}^{n+1}\sqrt{U^2+V^2}}{(H+\zeta)^2} + T^{(x)}{}_{i,j}^{n} \tag{23}$$

$$\frac{V_{i,j}^{n+1} - V_{i,j}^{n}}{\Delta t} = -\frac{f_V\left(U_{i,j}^{n+1} + \overline{U}_{i,j}^{n}\right)}{2} - \frac{rV_{i,j}^{n+1}\sqrt{U^2+V^2}}{(H+\zeta)^2} + T^{(y)}{}_{i,j}^{n} \tag{24}$$

Where f_U and f_V are the Coriolis terms at the positions of (U,V) in the Arakawa C mesh. Equations (23) and (24) can be written in the form

$$U_{i,j}^{n+1}R_{i,j}^{(x)n} - \hat{f}_U V_{i,j}^{n+1} = \tilde{U}_{i,j}^{n}$$

$$V_{i,j}^{n+1}R_{i,j}^{(y)n} + \hat{f}_V U_{i,j}^{n+1} = \tilde{V}_{i,j}^{n}$$

Or in matrix form

$$\begin{pmatrix} 1 & -\hat{f}_U \\ \hat{f}_V & 1 \end{pmatrix}\begin{pmatrix} U_{i,j}^{n+1} \\ V_{i,j}^{n+1} \end{pmatrix} = \begin{pmatrix} \tilde{U}_{i,j}^{n} \\ \tilde{V}_{i,j}^{n} \end{pmatrix} \tag{25}$$

Where

$$R_{i,j}^{(x)n} = 1 + \frac{r\sqrt{U^2+V^2}}{(H+\zeta)^2},\quad R_{i,j}^{(y)n} = 1 + \frac{r\sqrt{U^2+V^2}}{(H+\zeta)^2}$$

$$\hat{f}_U = \frac{\Delta t f_U}{2R_{i,j}^{(x)n}}, \quad \hat{f}_V = \frac{\Delta t f_V}{2R_{i,j}^{(y)n}}$$

$$\tilde{U}_{i,j}^{n} = \frac{1}{R_{i,j}^{(x)n}}\left(U_{i,j}^{n} + \frac{f_U \overline{V}_{i,j}^{n}}{2} + T^{(x)n}_{i,j} \right)$$

$$\tilde{V}_{i,j}^{(y)n} = \frac{1}{R_{i,j}^{(y)n}}\left(V_{i,j}^{n} - \frac{f_V \overline{U}_{i,j}^{n}}{2} + T^{(y)n}_{i,j} \right)$$

Considering the matrix $A = \begin{pmatrix} 1 & -\hat{f}_U \\ \hat{f}_V & 1 \end{pmatrix}$, its inverse $A^{-1} = \begin{pmatrix} 1 & \hat{f}_U \\ -\hat{f}_V & 1 \end{pmatrix}$ and its determinant $\det A = \left(1 + \hat{f}_U \hat{f}_V\right)$, the solution of (24) is then given by

$$\begin{pmatrix} U_{i,j}^{n+1} \\ V_{i,j}^{n+1} \end{pmatrix} = \frac{1}{\det A}\begin{pmatrix} 1 & \hat{f}_U \\ -\hat{f}_V & 1 \end{pmatrix}\begin{pmatrix} \tilde{U}_{i,j}^{n} \\ \tilde{V}_{i,j}^{n} \end{pmatrix}$$

Developing the matrix products and including the continuity equation, the following equations are obtained.

$$U_{i,j}^{n+1} = \frac{1}{\left(1 + \hat{f}_U \hat{f}_V\right)}\left(\tilde{U}_{i,j}^{n} + \hat{f}_U \tilde{V}_{i,j}^{n} \right) \qquad (26)$$

$$V_{i,j}^{n+1} = \frac{1}{\left(1 + \hat{f}_U \hat{f}_V\right)}\left(-\hat{f}_V \tilde{U}_{i,j}^{n} + \tilde{V}_{i,j}^{n} \right) \qquad (27)$$

$$\zeta_{i,j}^{n+1} = \zeta_{i,j}^{n} - \Delta t\left[\frac{u_{i,j+1}^{n+1} H_{i,j}^{(u)n} - u_{i,j}^{n+1} H_{i,j-1}^{(u)n}}{\Delta x} - \frac{v_{i,j}^{n+1} H_{i,j}^{(v)n} - v_{i+1,j}^{n+1} H_{i+1,j}^{(v)n}}{\Delta y} \right] \qquad (28)$$

The numerical solution of the horizontal equations of motion (26), (27) and continuity equation (28) satisfies the Courant, Friedrich, Lewy (CFL) criterion and the criterion for the inertial terms represented by equation (15) for numerical stability. The numerical simulations were applied to the Gulf of California. A mesh embracing the studied region with a grid resolution of 3 minutes (approximately 5560 m) generated a matrix of (179,177) and a total number of 7098 wet points.

To model the Lagrangian trajectories, a simple bilinear method of interpolation was applied on an Arakawa C mesh. An additional term representing a turbulent contribution to the horizontal components of the velocity, (u,v), was added. This turbulent contribution was generated with a Gaussian distribution with a maximum amplitude of 0.01 ms^{-1}. The middle point of every Arakawa C cell of the Gulf of California represented the initial position of 10 particles. To determine the final position of the Lagrangian trajectories, the averages $\bar{x}$ and $\bar{y}$ values were determined for every group of particles that initiated at every grid cell. The calculations were performed for a neap-spring tidal cycle considering seven tidal components (M_2, S_2, K_2, N_2, K_1, O_1, P_1). Since semidiurnal tides are dominant, the applied period for the Neap-spring tidal cycle was half a synodic month, i.e. 14.765 days. The synodic month is related to the phases of moon and is approximately 29.53 days. To calculate the Lagrangian residual current, the net displacements $\bar{x}$ and $\bar{y}$ were divided through the total time of simulation. In this way the components of the Lagrangian residual current were obtained for every grid point.

Results

The stability analysis of a semi-implicit approximation of the Coriolis terms led to the numerical solution described in the last section. To test the correctness and performance of the model, several numerical experiments were carried out. Several author have modeled diverse aspects of the principal lunar M_2 tide applying different numerical models (Stock, 1976; Quiros et al., 1992; Carbajal, 1993; Argote et al., 1995; Gutierrez et al., 2004). In Figure 2, the calculated

amphidromic system associated to the M_2 tidal constituent is shown. The amphidrome is quite similar to those calculated with other numerical models or obtained from measurements around the Gulf of California. Similar results were obtained for other tidal constituents (Table 1). The numerical model reproduces acceptably the behavior of tides in the Gulf of California.

Table 1. Observed (UNAM) and calculated amplitudes (m) and phases of several tidal constituents in the Gulf of California. Observed values above and calculated below.

Place	M2		S2		K1	
	A	P	A	P	A	P
Puerto Peñasco	1.57	59.0	0.945	58.9	0.431	80.9
	1.5	60.4	0.827	61.6	0.364	77.8
Bahía de los Ángeles	0.66	62.8	0.339	71.0	0.461	99.8
	0.65	63.3	0.361	65.5	0.31	79.9
La Paz	0.239	274.3	0.179	271.6	0.25	83.9
	0.222	257.4	0.178	253.8	0.224	78.5
Guaymas	0.136	311.9	0.106	286.6	0.279	73.7
	0.116	327.3	0.084	293.3	0.252	75.5
Yavaros	0.221	304.5	0.157	292.7	0.257	84.8
	0.18	279.3	0.148	267.3	0.237	74.9

It is known that tides in the Gulf of California belong to the most remarkable of the world. With high amplitudes of the sea surface elevation in the northernmost part of the gulf and strong tidal currents in the northern half. Although there is information about more tidal constituents, the seven applied components, (M_2, S_2, K_2, N_2, K_1, O_1, P_1), are the most important. Tidal current patterns (northwards and southwards) at different times of the calculation are shown in Figure 3. Taking into account that tidal waves can extend hundreds or thousands of kilometers from the

coast where the amplitude is a maximum and considering that the Gulf of California is a narrow sea, the presence of a dominant rectilinear motion, observed in Figures 3a and 3b, is explained. Only the coastal configuration and the presence of several islands in the archipelago region introduce some departures of the rectilinear flow. This rectilinear motion is intensified in the Colorado River Delta by a convergence process. Here arises the question if this dominant rectilinear flow in combination with a complex bathymetry and with some geographical irregularities generates a more sophisticated residual flow. The knowledge of residual currents in seas where the tides are dominant is important for the calculation of the transport of dissolved substances (pollution and sediments) and biological matter such as larvae, zooplankton, phytoplankton and microalgae. The Gulf of California is rich in processes involving transport of suspended matter. It has been recognized that residual currents at a fixed point (Euler residual current) is not enough to explicate completely residual currents. It is necessary to consider other dynamical properties through the Stokes and Lagrange residual currents. Longuet-Higgins (1969) found that the Lagrange residual current can be expressed as the sum of the Euler and Stokes (or Stokes' drift) residual currents.

The most calculated residual currents in studies on tidal dynamics is the Euler residual current. Due to its simplicity, it is usually calculated in studies of tides in shelf regions. It is defined as

$$u_{Euler} = \frac{1}{T}\int_{T} u dt \tag{29}$$

Additionally, the Stokes' residual current is calculated in the following way

$$u_{Stokes} = \frac{1}{HT}\int_{T} u\zeta dt \tag{30}$$

In a theoretical analysis on the mechanism of the Stokes drift, wei et al. (2004) found a similar expression to equation (30), but additionally a term that consider the interaction between topography, current and net displacement. This nonlinear interaction is not considered here. The question about the validity of the Lagrange residual current, calculated using Eulerian quantities, has been the subject of discussion in several research works. u_{Euler} and u_{Stokes} are Eulerian estimates because they are properties at a fixed point in space (Cheng and Casulli, 1982). Zimmerman (1972) showed that only under certain circumstance the relation $u_{Lagrange} \approx u_{Euler} + u_{Stokes}$ is valid, specifically if the amplitude of the displacement of the oscillatory flow is small in comparison with the variability of the velocity field. According to Meier-Reimer (1977), the Lagrange residual current, $u_{Lagrange}$, satisfies the relationship, $u_{Lagrange} \approx u_{Euler} + u_{Stokes}$, in good approximation in seas. Quan et al. (2014) demonstrated that the Lagrange residual current is proven to be a more suitable description of residual currents than any other residual velocity. In this research work, different numerical experiments were carried out to calculate the Lagrange residual current; first as the sum of the Euler and Stokes residual currents and later using Lagrangian trajectories. Another major aim of this research work was to examine the possible generation of a rectification process of tidal currents by the presence of islands in the central part of the Gulf of California.

The applied trajectories to calculate the Lagrangian residual currents were simulated in the following way: the middle point of every Arakawa C cell of the Gulf of California represented the initial position of 10 particles. After the time of simulation, from the final position of the 10 particles, a middle position was calculated. Since the time of simulation is known, it enables the estimation of the horizontal components of the velocity vector. In Figure 4, the Lagrange residual current, obtained for the M_2 tidal constituent, is displayed for the northern half of the Gulf of California. Residual currents in the southern part are very small. Several eddies, cyclonic and anticyclonic, can be distinguished in the northern part of the

gulf. Several regions with relatively strong residual currents are found in the transition zone (archipelago region) from very deep zones to shallower areas. The structure of the Lagrangian residual currents of the M_2 tide serves as a reference for the comparison with residual currents considering several tidal constituents.

Considering seven tidal constituents (M_2, S_2, K_2, N_2, K_1, O_1, P_1), the Lagrange, Euler and Stokes residual currents were also estimated for a neap-spring tidal cycle, i.e. 14.765 days or half a synodic month. For the calculation of the Lagrange residual current, $u_{Lagrange}$, trajectories of particles were considered as it has been commented above. u_{Euler} and u_{Stokes} were calculated applying the equations (29) and (30). These two residual currents are shown in Figure 5. Comparison of the Lagrange residual current caused by the M_2 tide (Figure 4) with the Euler residual current for the neap-spring cycle considering the tidal constituents (M_2, S_2, K_2, N_2, K_1, O_1, P_1) (Figure 5a) reveals that the residual patterns are quite similar. It is an indication that residual currents are highly dependent on the geometry of the basin (bathymetry and coastal configuration). Although the residual current patterns are quite similar, the intensity of residual currents is significantly larger with seven tidal constituents. It is worth mentioning the strong cyclonic gyre over the Salsipuedes sill, on the west side of the archipelago region. In the Colorado River Delta, a relatively strong cyclonic gyre and an anticyclonic circulation appear in the Euler residual current. In Figure 5b, the Stokes residual current, calculated according to equation (30), is shown. The Stokes residual current is important in the shallow areas of the Colorado River Delta, in the Adair Bay and San Carlos Bay and in the Infiernillo Channel. In these regions, the residual current reaches values varying between 0.01 and 0.015 ms^{-1}. It is worth mentioning that in the Infiernillo Channel, the Stokes residual current (Figure 5b) is southwards whereas in the Euler residual current (Figure 5a) the flow is dominantly northwards.

Once the Euler and the Stokes residual currents were estimated applying equations (29) and (30) for a neap-spring tidal cycle, the following step was to estimate the Lagrange residual current. The Lagrange residual current, obtained using the equation, $u_{Lagrange} \approx u_{Euler} + u_{Stokes}$, is shown in Figure 6a. It can be compared with the Lagrange residual current calculated using trajectories which is shown in Figure 6b. Both patterns are quite similar, with the same gyres in the northern part of the Gulf of California and with the same order of magnitude. It is evident that the corrections introduced by the Stokes residual current (Figure 5b) in the areas of the Colorado River Delta, in the Adair Bay and in the Infiernillo Channel appear in both calculations of the Lagrange residual current. The Lagrange residual current reaches values ranging between 0.01 and 0.03 ms^{-1} in the area of the Colorado River Delta. On the west side of this area, a strong cyclonic residual circulation develops. A couple of gyres, one of them cyclonic and the other one anticyclonic, develops in the central part from a northwards current. A relatively strong tidal residual current appears to the south of Tiburon Island, i.e. in the transition zone from deep to shallower regions. Another interesting result is that along the east coast of the gulf, the residual current is dominantly southwards whereas along the west coast the flow is northwards. From the southern part of the archipelago region until the Colorado River Delta in the northernmost part of the gulf there is a meandering residual current produced by the seven tidal constituents (M_2, S_2, K_2, N_2, K_1, O_1, P_1). Although it is not shown, it is worth mentioning that tidal residual currents are very small in the southern half of the Gulf of California, only in the shallow areas of the eastern coast is the residual current of some significance.

Discussion

It is known that in some sea areas of the world, the neap-spring tidal cycle is modulated by the synodic month, i.e. by moon phase changes. The synodic neap–spring cycles occur when the M_2 and S_2 tidal constituents come into phase or out of phase (Pugh, 1987). Not all neap-spring tidal cycles are determined by a period

of 14.765 days, i.e. half a synodic month. There are basins in which the neap-spring tidal cycle is driven by half a tropical month (13.66 days), like in the Gulf of Mexico (Kvale, 2006). This neap-spring cycle is generated by the tidal constituents K_1 and O_1. In the Gulf of California, the M_2 and S_2 tidal constituents are in phase every 14.765 days. In the northern part of the gulf, the relative importance of tides like the K_1 and O_1 has been often considered as small. In Figure 7, time series of the sea surface elevation at a point in the area of the Colorado River Delta, is shown. Whereas the combination of the M_2 and S_2 tidal constituents generate amplitudes of about 3 m, the tidal constituents K_1 and O_1 produce amplitudes of about 0.5 m. Observe that the neap-spring tidal cycle is different for these two numerical experiments and that the influence of the tidal constituents K_1 and O_1 is important. To calculate the Lagrange, Euler and Stokes residual currents, a period of 14.765 days was applied. The most important characteristics of the Euler, Stokes and Lagrange residual currents have been described previously, emphasizing the generation of several gyres, some of them in pairs. Another important result is a continuous and meandering current with velocities varying between 0.01 and 0.02 ms^{-1} which extends from the transition zone, from deep to shallower regions in the southern part of Tiburón Island, until the Colorado River Delta in the northernmost part of the gulf. These residual currents of about 0.02 ms^{-1} would transport a passive tracer a distance of about 1730 m in a day, or about 50 km in a month.

The analysis of the Euler, Stokes and Lagrange residual currents has also revealed another interesting process in the archipelago region. In Figure 8a, on the east side of Tiburon Island (Infiernillo Channel) there is a northwards Euler residual current with values of about 0.008 ms^{-1}. Just the opposite, i.e. a southwards flow occurs in the Stokes residual current shown in Figure 8b. The velocity values for this residual current are of the order of 0.01 ms^{-1}. This stronger southwards flow overlaps the Euler residual current as it can be seen in Figure 8c where the Lagrange residual current is displayed. The Euler and Stokes residual current were

calculated according to the equations (29) and (30) respectively. The Lagrange residual current was estimated using trajectories of particles that initiated the displacement in the middle of every grid cell. This result indicates that from the superposition of the Euler and Stokes residual currents arises a rectification process of the oscillating tidal flow around Tiburón Island where an anticyclonic circulation is generated (Figure 8c). It is important to mention that this rectification process is observed both in the sum of Euler and Stokes residual currents and in the Lagrange residual current calculated with particle trajectories. The rectification process is not so obvious around Angel de la Guarda Island. An anticyclonic circulation occurs in almost three quarters of the length around the island. At the southern side, the presence of a relatively strong northwards flow inhibits the complete anticyclonic circulation around Angel de la Guarda. The rectification of oscillating tidal flows has been explained in several forms (Zimmerman, 1978; Loder, 1980). Continuity, Coriolis effects and bottom friction play a relevant role in the rectification mechanism (Huthenance 1973). Zimmerman (1978) asseverated that Coriolis and frictional torques caused by a variable bottom bathymetry, produce a vorticity field that is transferred to the mean flow by the non-linear advection terms. Loder (1980) explained the rectification process as an interaction of the mean flow and the oscillating tidal currents in a topographic gradient. In this research work, to explain the rectification of tidal currents by the presence of Tiburón Island use is made of the Euler, Stokes and Lagrange residual currents. Loder (1980) called the attention about the importance of the Stokes residual current in the rectification process. The clockwise sense of rotation of the circulation around Tiburón Island in the Gulf of California is the same as that calculated and observed in Georges Bank, in the neighborhood of the Gulf of Maine, on the west coast of the North Atlantic Ocean.

To estimate the Lagrange residual currents was necessary to calculate trajectories of particles. This was carried out applying a bilinear method to interpolate the horizontal components of the vector velocity in an Arakawa C mesh. The

Lagrangian trajectories of particles were calculated at different points in the northern part of the Gulf of California and for distinct combinations of tidal constituents. The principal interest was to visualize the influence of the geometry of the basin on the trajectories. Pure Kelvin waves exhibit a rectilinear motion along an ideal rectilinear coast. Although this condition is not met in real seas, the oscillating tidal flow is often almost rectilinear close to the coast (on the right side of a propagating Kelvin wave in the northern hemisphere). The presence of embayment may generate Poincare waves with an increase of the eccentricity of the tidal ellipses. From this discussion, nearly rectilinear flow or ellipses with a small eccentricity are expected in the neighborhood of the coasts. Since the exponential decay of Kelvin waves is not the same for the different tidal constituents, far away from the coast the relative amplitude values changes. Another geometrical factor that may influence the Lagrangian trajectories is the presence of islands, like in the archipelago region, in the central part of the Gulf of California. In Figure 9, the Lagrangian trajectories generated by the M_2 tide in the northern part of the Gulf of California are shown. The trajectories are displayed for the time equivalent to 5 M_2 periods, i.e. about 62.1 hours. At the points A, B, C, E and F, the eccentricity of the ellipses is small. These points are located in the neighborhood of coasts. The coastline imposes restrictions on the flow according to the property of Kelvin waves of a rectilinear flow. The reflection process of the Kelvin wave, described by Taylor (1921), imposes also conditions on the eccentricity of tidal ellipses. It is interesting to note that the residual current at F is very small. This can be corroborated in Figures 5 and 6 where the Euler, Stokes and Lagrange residual currents are very small in that area. At point H, the ellipses are not deformed and the eccentricity of the ellipses is small. At points D and G, the ellipses are strongly distorted. Point D is located in a convergence zone of several flows with a relatively strong Lagrange residual current. The clockwise circulation around Tiburón Island, produced in the rectification process, exhibits a flow in the northwest direction in the area of point G. The net displacement of this particle reflects this fact. Since the point G is located in an area with variable

residual currents, the trajectories have a complicated form and they do not describe closed ellipses.

When several tidal constituents are considered in the calculation of Lagrangian trajectories, the paths followed by the particles is much more complex. Since the exponential decay of Kelvin waves is not the same for the different tidal constituents, far away from the coast the relative amplitude values changes. This may lead to complex trajectories. Another geometrical factor that may influence the Lagrangian trajectories is the presence of islands, like in the archipelago region, in the central part of the Gulf of California. The phase differences may also play a role in the complexity of trajectories of particles. Although the Gulf of California is a narrow sea, the Lagrangian trajectories are far from a rectilinear motion. The presence of a complex geometry, coasts and bathymetry evenly contribute to this intricacy of particle trajectories. In Figure 10, the trajectories of the particles reflect the fact that there is a transition from neap to spring tides, i.e. the amplitudes tend to be larger. As in the case of the M_2 tide, at point G the particle trajectory in that area is very complicated. In the very shallow area of the Colorado River Delta, the trajectory at point A is also complex. The initial point (triangles) and the end point (black circles) reflect the tendency of the Lagrangian residual currents. It is remarkable that no matter the complicated trajectories of water particles, as shown in Figure 10, the net effect of these trajectories leads to a smooth behavior of residual currents. Finally, the strong rectilinear tidal currents are rectified by the geometry of the basin producing a net clockwise circulation around Tiburon Island and a series of clockwise and anticlockwise gyres in the Northern Gulf of California.

Conclusions

In this research work, a detailed study have been carried out of residual currents in the Northern Gulf of California. The Lagrangian residual current for the M_2 revealed

several cyclonic and anticyclonic gyres. When the calculation considered several tidal constituents (M_2, S_2, K_2, N_2, K_1, O_1, P_1), the Euler, Stokes and Lagrange residual currents were calculated. The structure of the Euler and Lagrange residual currents were quite similar to that of the M_2 alone, but the intensity of currents was larger. It indicates that residual currents are strongly influenced by the geometry of the basin and by friction. In fact, all calculated gyres can be considered as the result of a rectification process. The periods considered in the calculations were 12.4206 hours for the M_2 and 14.765 days for the neap-spring tidal cycle. The Stokes residual current revealed relative high values only in several zones of the northern part of the gulf, particularly in the Colorado River Delta, in the bays of Adair and San Carlos and in the Infiernillo Channel. Euler and Stokes residual currents are quite different, but the superposition of them determines a more realistic picture of residual currents. For example, it has been demonstrated that around Tiburon Island, the observed rectification of tidal currents is explained by the superposition of the Euler and Stokes residual currents. This rectification process generates an anticlockwise circulation around Tiburón Island. In fact, the Lagrange residual currents can be obtained from the addition of the Euler and Stokes residual currents. Since the Lagrangian residual currents, obtained from Lagrangian trajectories, is practically the same, the rectification process is also observed in this calculation. Although the Gulf of California is a narrow sea, the Lagrangian trajectories of particles at different positions can be very complex.

Referencias

Argote M.L., A. Amador, M.F. Lavín, J.R. Hunter, 1995. Tidal dissipation and stratification in the Gulf of California. Journal of Geophysical Research, 100, 16, 103-16, 118.

Carbajal, N., 1993. Modelling of the circulation in the Gulf of California. Ph.D. Thesis,University of Hamburg, Germany 186 pp.

Carbajal, N., Backhaus, J.O., 1998. Simulation of tides, residual flow and energy budget in the Gulf of California. Oceanololica Acta. 21, 429–446.

Carbajal N., Montaño Y., 2001. Comparison between predicted and observed physical features of sandbanks. Estuarine Coastal and Shelf Science, 52, 435-443.

Cheng R.T. and Casulli V., 1982. On Lagrangian residual currents with applications in south San Francisco Bay, California. Water Resources Research, Volume 18, Issue 6, pages 1652 1662.

Filloux J.H., 1973. Tidal patterns and energy balance in the Gulf of California, Nature 243 (1973) 217-221.

Fu L.L. and Holt B., 1984. Internal waves in the Gulf of California: Observations from a spaceborne radar. Journal of Geophysical Research, Vol. 89, No. C2, pages 2053-2060.

Grijalva N., 1972. Tidal computation in the Gulf of California. Geofísica Internacional, Volumen 12, No. 2, pp. 13-34.

Gutiérrez O.Q., Marinone_S.G., Parés-Sierra A., 2004. Lagrangian surface circulation in the Gulf of California from a 3D numerical model. Deep Sea Research II, 51, 659–672.

Hendershott M.E. and Speranza A., 1971. Co-oscillating tides in long, narrow bays: The Taylor problem revisited, Deep Sea Res., 18, 959-980.

Hernández-Azcúnaga L., Carbajal N. and Montaño-Ley Y., 2013. Bedload Transport of sediments and morphodynamics in the Northern Gulf of California. Journal of Coastal Research, Vol. 30, Issue 2, 228-236.

Huthnance J.M., 1973. Tidal current asymmetries over the Norfolk Sandbanks. Estuarine and Coastal Marine Science, Volume 1, Issue 1, Page 89-99.

Kvale E.P., 2006. The origin of neap–spring tidal cycles. Marine Geology, Volume 235, Issues 1–4, 20, Pages 5–18.

Loder J.W., 1980. Topographic rectification of tidal currents on the sides of Georges Banks. Journal of Physical Oceanography, 10(9), 1399-1416.

Longuet-Higgins M.S., 1969. On the transport of mass by time-varying ocean currents. Deep Sea Research, Vol. 16, pp. 431-447.

Maier-Reimer E., 1977. Residual circulation in the North Sea due to the M2-tide and mean annual wind stress. Dt. Hydrogr. Z. 32 (1977) 126-130.

Marinone S.G. and Lavín F.M., 2003. Residual current and mixing in the large islands region of the central Gulf of California. In Non-linear processes in geophysical fluid dynamics 213-236, O.U. Velasco Fuentes et al. (Eds) Kluwer Academic Publisher.

Montaño Y. and Carbajal N., 2008. Numerical experiments on the long term morphodynamics of the Colorado River Delta. Ocean Dynamics, 58, 19-29.

Morales, R.A. and Gutiérrez G., 1989. Mareas en el Golfo de California, Geofísica Internacional, Vol. 28-1, pp. 25-46.

Pugh, D.T., 1987. Tides, Surges and Mean Sea Level. John Wiley and Sons, New York. 472 pp.

Quiros, G., Badan-Dangon A., Ripa P., 1992. M2 Currents and residual flow in

the Gulf of California. Netherlands Journal of Sea Research 28(4), p. 251-259.

Salas de León D.A., Carbajal N, Monreal-Gómez M.A. and Gil-Zurita A., 2011. Vorticity and mixing induced by the barotropic M2 tidal current and zooplankton biomass distribution in the Gulf of California. Journal of Sea Research, 66, 143–153.

Salas de León D.A., Carbajal-Pérez N., Monreal-Gómez M.A. and Barrientos MacGregor G., 2003. Residual circulation and tidal stress in the Gulf of California. Journal of Geophysical Research, Vol. 108, No. C10, 3317, doi:10.1029/2002JC001621.

Stock, G.G., 1976. Modelling of tides and tidal dissipation in the Gulf of California, Ph.D. thesis, 102 pp., Scripps Inst. of Oceanography, Univ. of Calif., San Diego.

Taylor G.I., 1921. Tidal oscillations in Gulfs and rectangular basins. Proceedings of the London Mathematical Society, 20, 148-181.

Zimmerman J.T.F., 1978. Topographic generation of residual circulation by oscillatory (tidal) currents. Geophysical and Astrophysical Fluid Dynamics, 11, 35-47.

CAPTIONS

Figure 1. Bathymetry of the Gulf of California. The position and names of relevant zones are shown. The box indicates the geographical region and the small square specifies the studied northern part of the gulf.

Figure 2. M_2 tidal amphidromic system in the Gulf of California. The phases are referenced with respect to the phase in Cabo San Lucas at the entrance to the Gulf of California which considered as zero.

Figure 3. Instantaneous tidal currents at two different times to show the northwards (a) and southwards (b) flow patterns. The box indicates the studied part of the Gulf of California.

Figure 4. Lagrange residual current for the M_2 tide. The residual current was estimated using Lagrangian trajectories.

Figure 5. Euler residual current (a) and Stokes residual current (b). The residual currents were calculated for a neap-spring tidal cycle.

Figure 6. Lagrange residual current calculated from the sum of the Euler and Stokes residual currents (a). Lagrange residual current calculated using trajectories (b). The calculations were carried out for a neap-spring tidal cycle.

Figure 7. Time series of the sea surface elevation at a point in the Colorado River Delta. Considering the tidal constituents M_2 and S_2 (a). Simulation considering the tidal constituents K_1 and O_1 (b). Consideration of the tidal constituents M_2, S_2, K_1 and the O_1 (c). Observe that the neap-spring tidal cycle is not the same in (a) and (b).

Figure 8. Residual currents applying the tidal constituents M_2, S_2, K_2, N_2, K_1, O_1, P_1. (a) Euler residual current. (b) Stokes residual current. (c) Lagrange residual current as the superposition of Euler and Stokes residual currents. The rectification process (thick arrows) is evident around Tiburon and Angel de la Guarda Islands as a clockwise circulation.

Figure 9. Lagrangian trajectories of particles in different zones of the northern part of the Gulf of California. The trajectories were calculated considering the tidal constituents M_2. Triangles indicate the starting point.

Figure 10. Lagrangian trajectories of particles in different zones of the northern part of the Gulf of California. The trajectories were calculated considering the tidal constituents (M_2, S_2, K_1, O_1, N_2). Triangles indicate the starting point.

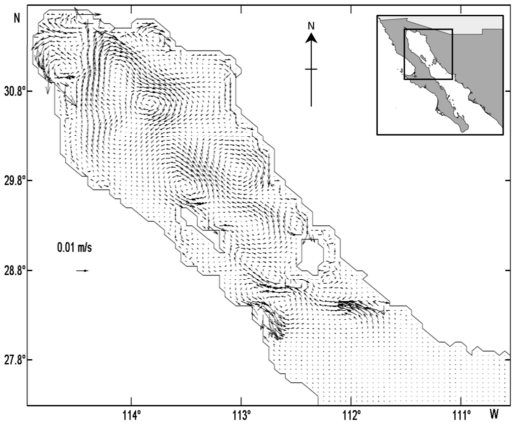

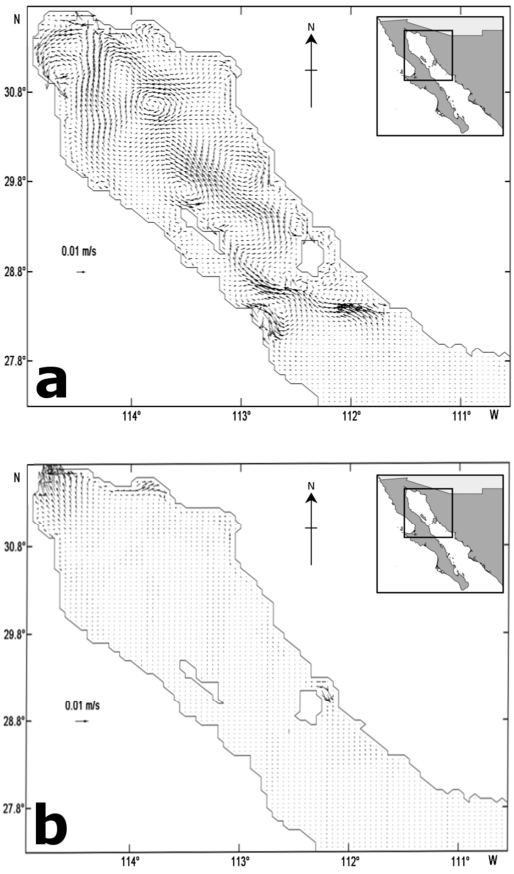

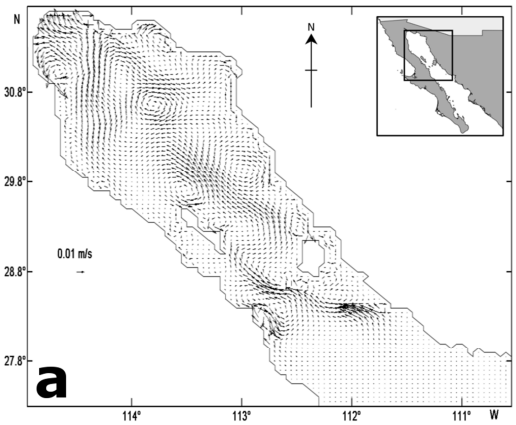

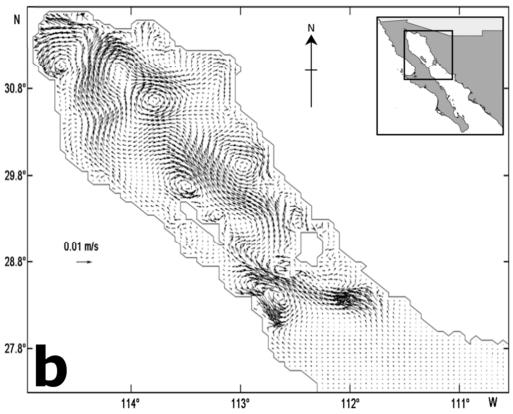

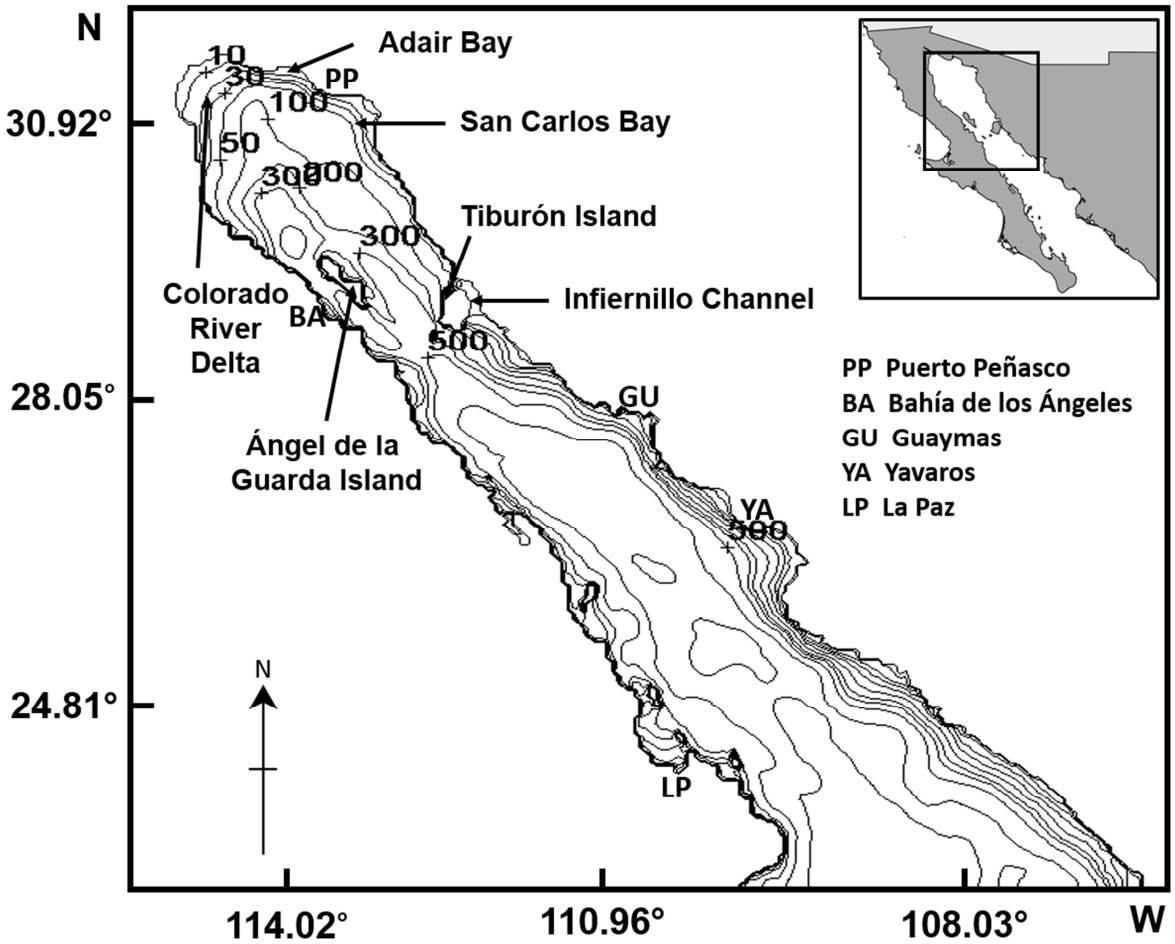
N
30.92°
28.05°
24.81°
114.02°
110.96°
108.03°
W
Adair Bay
PP
San Carlos Bay
Tiburón Island
Infiernillo Channel
Colorado River Delta
BA
Ángel de la Guarda Island
GU
YA
LP
10
30
100
50
300
500
PP Puerto Peñasco
BA Bahía de los Ángeles
GU Guaymas
YA Yavaros
LP La Paz